Journal of the Geological Survey of Brazil

The Paleoproterozoic metaconglomerate-hosted Castelo de Sonhos gold deposit, Tapajós Gold Province, Amazonian Craton: a modified paleoplacer origin

Joana D'Arc da Silva Queiroz[1,2], Evandro L. Klein[3,1]

[1] GPGE – Grupo de Pesquisa em Geologia Econômica, PPGG – Programa de Pós-Graduação em Geologia e Geoquímica, Universidade Federal do Pará. Rua Augusto Corrêa, 1 – Guamá. Belém, PA, Brazil. CEP 66075-110.
[2] SEMAS – Secretaria de Estado de Meio Ambiente e Sustentabilidade, Belém, Brazil.
[3] CPRM-Geological Survey of Brazil. SBN, Quadra 02, Bloco H, 1° andar, Brasília-DF, CEP: 70040-904.

Abstract

The Castelo de Sonhos gold deposit (~1.5 Moz Au) is located in the southeastern Tapajós Gold Province and is hosted in variably deformed metaconglomerates and metasandstones of the Castelo dos Sonhos Formation, which was deposited between 2011 and 2050 Ma and considered to be a relic of a major foreland system. Gold is found mainly in the matrix of metaconglomerates and subordinately in fractures of metasandstones. The host rocks are strongly silicified, which was demonstrated to be the result of silica overgrowth during diagenesis, without relationship to hydrothermal alteration. The rocks are also impregnated with secondary iron oxides, which are interpreted to be consequence of weathering of the metasedimentary sequence and total or partial dissolution of iron-bearing minerals and re-precipitation of iron during circulation of oxidized (meteoric and/or magmatic) fluids. The morphology of matrix gold particles indicates that they are not pristine, but only slightly modified and reshaped, which suggests detrital provenance and relatively proximal distance of transport from the original sources. The chemical composition of the particles, with Au grading 94-97%, very high Au/Ag and lack of other significant metals, suggest single source, or sourcing from a single class (orogenic?) of gold deposits. The gold particles from fractures are platy and show even higher Au/Ag ratios, given by very low Ag contents (<<1%), which are interpreted as epigenetic remobilization of the matrix gold. Oxygen isotope compositions of hydrothermal quartz-sulfide-muscovite veins cutting across the host metasedimentary sequence indicate magmatic origin for the fluids, which might have been produced by granites that intruded the metasedimentary rocks and helped gold remobilization to fractures. As a consequence, Castelo de Sonhos is interpreted as a modified paleoplacer gold deposit.

Article Information

Publication type: Research paper
Submitted: 29 May 2018
Accepted: 15 August 2018
Online pub. 25 August 2018
Editor(s): Carlos Spier

Keywords:
gold, quartz-pebble,sediment-hosted, metallogenesis, syngenesis, remobilization

*Corresponding author
Joana D'Arc da Silva Queiroz
E-mail address:
joana.ddqueiroz@gmail.com

1. Introduction

Gold deposits hosted in conglomerates are commonly found in Precambrian terranes worldwide, and a strong debate exists concerning the syngenetic, i.e., paleoplacer, versus modified paleoplacer and epigenetic origin of gold mineralization (see reviews in Law and Phillips 2005; Frimmel 2014). Deposits of this type are also present in Brazilian Precambrian terranes, occurring in cratonic areas and in more or less reworked Archean-Paleoproterozoic basement segments within Neoproterozoic mobile belts (Fig. 1). The same genetic issues apply to these Brazilian deposits, with Moeda and Serra da Jacobina, in the São Francisco Craton (Fig. 1), being the classic examples, and with Jacobina showing past production plus mineral resources in excess of 370 t of gold (Renger et al. 1988; Lecuyer and Moore 2009; Marques 2016).

The conglomerate-hosted Castelo de Sonhos gold deposit, located in the southeastern portion of the Tapajós Gold Province of the Amazonian Craton (Fig. 1), is a relatively recent discovery (Yokoi et al. 2001). The deposit is hosted in the Paleoproterozoic siliciclastic Castelo dos Sonhos Formation, deposited between 2011 and 2050 Ma (Klein et al. 2017), and shows indicated plus inferred resources of 1.5 Moz Au (46.5 t Au, Tristar Gold 2018), whereas unofficial past production from alluvial sediments of creeks that drain the host formation is estimated at 9.3 t Au (Appleyard et al. 2016).

A modified paleoplacer model has previously been proposed for the origin of the Castelo de Sonhos gold deposit (Santos et al. 2001; Mello 2014; Appleyard et al. 2016; Srivastava et al. 2016; Vargas and Campbell-Hicks 2017), and silicification and hematite alteration have been described as potential guides for mineralization (Mello 2014; Srivastava et al. 2016). However, nothing has been demonstrated about what kind of process (structural, hydrothermal, metamorphic, magmatic) has modified the assumed original detrital mineralization, and what has produced the supposed hydrothermal alteration.

In this contribution, we assess the proposed model, based on the mesoscopic and microscopic characteristics of the host

https://doi.org/10.29396/jgsb.2018.v1.n2.3
ISSN: 2595-1939

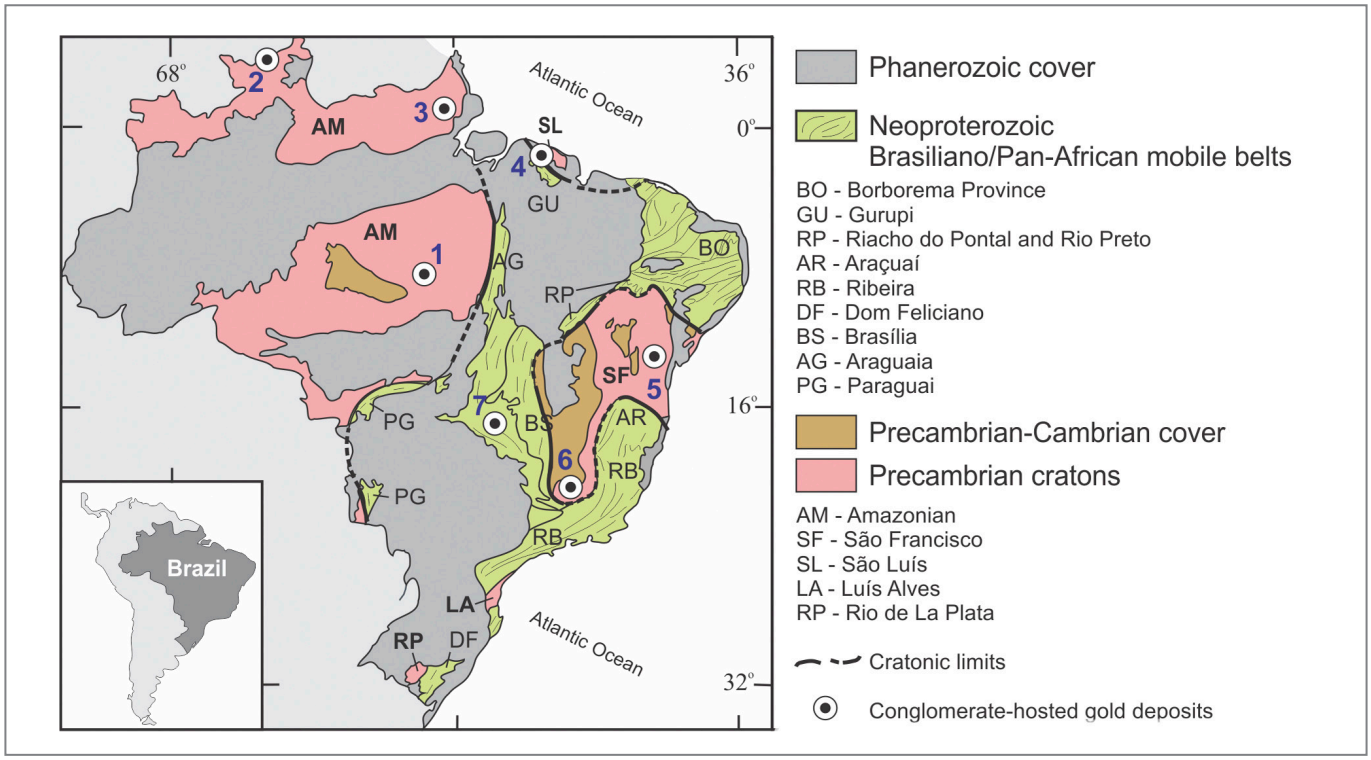

FIGURE 1 - Major tectonic units of Brazil with the location of (1) Castelo de Sonhos and other conglomerate-hosted gold deposits: 2 – Roraima, 3 – Vila Nova, 4 – Igarapé de Areia, 5 – Jacobina, 6 – Moeda, 7 – Faina.

rocks, along with the study of the morphology and chemical composition of gold particles. Additionally, reconnaissance studies of the chemical composition of white mica and of stable isotope compositions of quartz veinlets that cut across the mineralized strata were performed in order to constrain potential sources of hydrothermal modification of the paleoplacer.

2. Tapajós Gold Province

The Tapajós Gold Province consists of a large volcano-plutonic belt with subordinate metamorphic and sedimentary rocks (Fig. 2). The orogenic period, which spans from 2.03 Ga to 1.95 Ga, was preceded by the deposition of the Castelo dos Sonhos Formation (see next section), and started with the formation of subduction-related associations, represented by gneisses and granitoids of the Cuiú-Cuiú Complex (2033 to 2005 Ma), formed in continental arc. This complex is associated with the metavolcano-sedimentary Jacareacanga Group (<1972 Ma), and with undeformed and unmetamorphosed calc-alkaline felsic to intermediate volcanic and pyroclastic rocks of the Comandante Arara Formation (Santos et al. 2004; Vasquez et al. 2017 and references therein). The metamorphic units were intruded by batholiths of high-K, calc-alkaline granites of the Creporizão Intrusive Suite (1997 to 1956 Ma), and covered by felsic to intermediate volcanic and volcanoclastic rocks of the Vila Riozinho Formation. Both units show field and geochemical characteristics of mature magmatic arc to post-collision rock associations (Lamarão et al. 2002; Santos et al. 2004; Guimarães et al. 2015; Vasquez et al. 2017).

After a time gap of ca. 50 Ma, other plutonic-volcanic events have taken place in the Tapajós Gold Province. These started with the intrusion of calc-alkaline tonalite to granite of the Tropas Intrusive Suite (1907 to 1892 Ma), and of voluminous batholiths and stocks of high-K calc-alkaline granodiorite and subordinate tonalite and granite of the Parauari Intrusive Suite (1883 to 1879 Ma) and coeval gabbros (Santos et al. 2004; Vasquez et al. 2017 and references therein). The tectonic setting of this voluminous magmatism is equivocal, and both continental arc (Santos et al. 2004; Juliani et al. 2015) and extensional/intracontinental (Vasquez et al. 2008; Klein et al. 2017) settings have been proposed.

A large intracontinental rift system developed from ca. 1895 Ma onward and was filled by alkaline volcanic and pyroclastic rocks of the Iriri Group (1895 to 1864 Ma), which were intruded by the coeval alkaline granites of the Maloquinha Intrusive Suite (Santos et al. 2004; Vasquez et al. 2008). The clastic/volcanoclastic sediments of the Novo Progresso Formation (<1840 Ma, Klein et al. 2018) are also associated with this event, which is ascribed to the formation of the Uatumã Silicic Large Igneous Province (Klein et al. 2012 and references therein). This event was followed by the establishment of continental Statherian sedimentary basins and associated alkaline intracratonic magmatism.

3. Summary of the geology of the Castelo dos Sonhos basin

The Castelo dos Sonhos Formation consists of a metasedimentary sequence (Fig. 3A) and forms a broadly circular (15 x 12 km) plateau with maximum thickness in the central portion of the basin of about 1000-1100 m (Mello 2014). From the base to the top (Fig. 4A), the metasedimentary sequence is composed of the following strata (Alkmin 2011; Klein et al. 2017; Vargas and Campbell-Hicks 2017). (1) The >500 m-thick lower metasandstone layer comprises coarse-

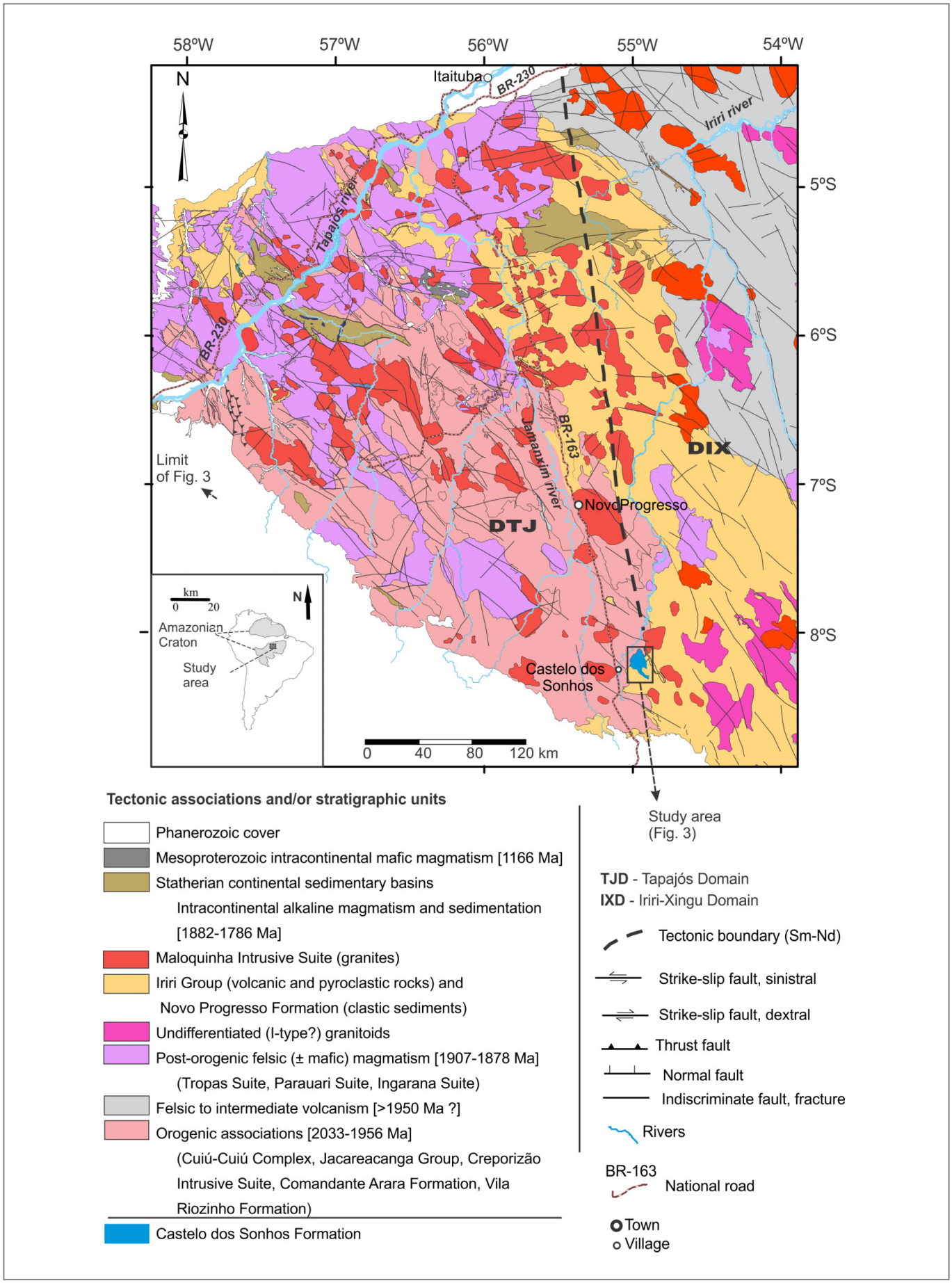

FIGURE 2 - Simplified geological map of the Tapajós Gold Province (adapted from Vasquez et al. 2008 and Klein et al. 2017).

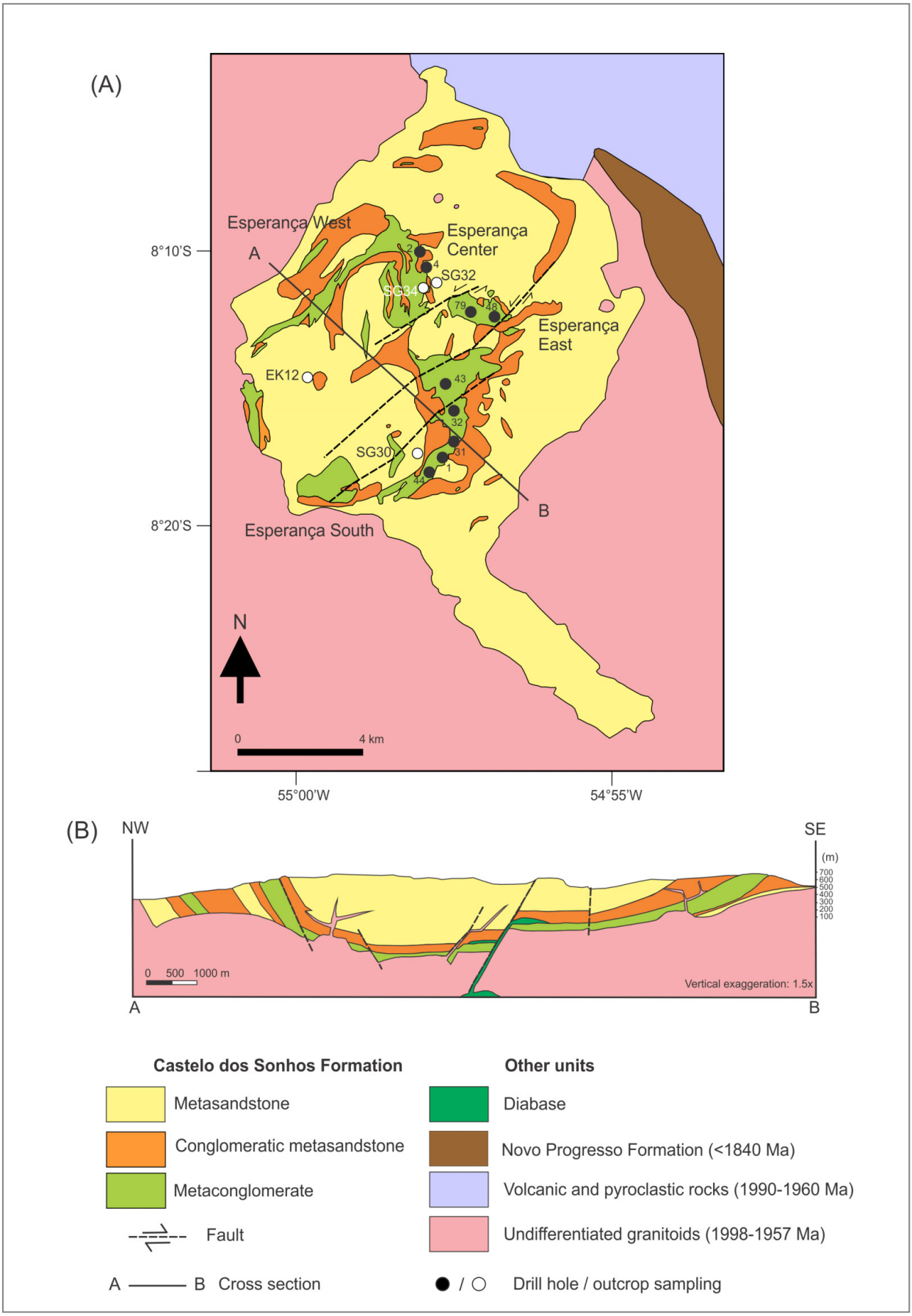

FIGURE 3 - (A) Geological map of the Castelo dos Sonhos Formation (modified from Mello 2014) and the surrounding area (adapted from Guimarães et al. 2015), with location of the mineralized targets (Tristar Gold 2018) and of the drill holes and outcrops sampled for this study (see also Appendix A for coordinates of the samples). (B) NW–SE cross section.

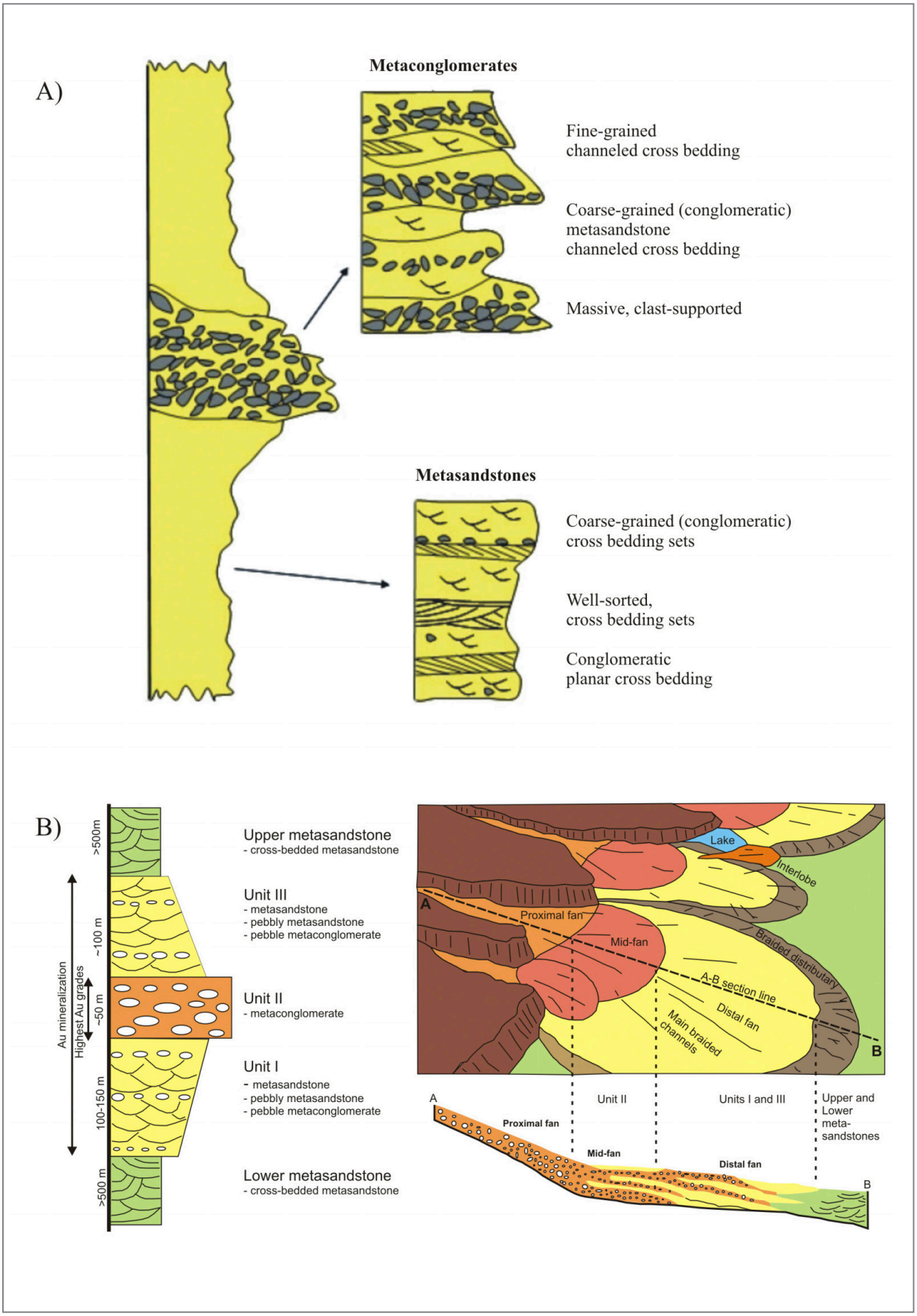

FIGURE 4 – (A) Simplified, not to scale, sedimentary section of the Castelo dos Sonhos Formation (adapted from Alkmin 2011). (B) Schematic section of part of the Castelo dos Sonhos Formation, with a more detailed subdivision of the central metaconglomerate layer and interpretation of the sedimentary setting (adapted from Karpeta 2016 apud Vargas and Campbell-Hicks 2017).

grained to conglomeratic (pebbly) metasandstones with planar cross bedding. (2) The 200 to 300 m-thick central layer of metaconglomerates, with channeled cross bedding. (3) The upper metasandstone layer, comprising a set of >500 m-thick of metasandstones and magnetite-rich metasandstones with large-scale cross bedding.

The central metaconglomerate layer was subdivided (Karpeta 2016 apud Vargas and Campbell-Hicks 2017) into three units (Fig. 4B). Units I and III (100-150 m-thick each) are composed of alternating metasandstone, pebbly metasandstone, and pebble metaconglomerate, occurring at the base and on the top of the Unit II, which consists of ca. 50 m-thick metaconglomerate, both matrix- and clast-supported, with granules (~2 mm), pebbles, cobbles and boulders of (~1 m). The cobbles appear to be smaller and less frequent to the top (see more detailed descriptions of the metaconglomerates and metasandstones in section 5.1).

According to Alkmin (2011) the facies associations show gradational contacts. These characteristics were attributed by Vargas and Campbell-Hicks (2017) to the influence of sediment deposition rate, distance to the eroded source, and the maturity (size, roundness, and sorting) of the sediments.

Structurally, the plateau presents a synformal configuration (Fig. 3B), with axis plunging 15-20° to SW. The southern limb (Esperança South target) is oriented to NE-SW/30-35°NW, the eastern limb (Esperança East target) is oriented to N-S, with dips of 30-35° to the West, whereas the north/northwestern limbs (Esperança Center and west targets) strikes NE-SW and dips 60-80° to SW (Alkmin 2011). The deformation of the rocks during the folding event imparted the observed preferential orientation of white mica crystals and of quartz pebbles, flattening of quartz pebbles, and produced late sinistral reverse shear zones defined by 20 cm-thick mylonite bands oriented to N56°W, with dips of 75° to SE. The ductile deformation was followed by brittle event that produced fractures and faults with variable orientations, including strike-slip faults that displaced the Esperança East target to the northeast (Fig. 3A).

The sedimentary setting of deposition of the Castelo dos Sonhos Formation was interpreted to be continental and related to a braided fluvial system associated with alluvial fans and subordinate aeolian dunes (Alkmin 2011; Klein et al. 2017), or to a fluvio-deltaic system (Srivastava et al. 2016; Vargas and Campbell-Hicks 2017). Accordingly, the clast- and matrix-supported metaconglomerates (Unit II) represent and intermediate fan, whereas the alternating metasandstones and metaconglomerates of Units I and III were deposited in a distal fan (Fig. 4B).

Provenance study show detrital zircons with ages spanning in time from 2050 to 3700 Ma and indicates that the source of detritus are Rhyacian and Archean terranes positioned to the east, northeast and southeast of the Tapajós Gold Province (Klein et al. 2017). Despite deformation, the cross-bedding in the metasandstones and the imbrication of pebbles in the metaconglomerates suggest that the paleo-current was from the northeast to the southwest (present-day configuration) (Karpeta 2016, apud Vargas and Campbell-Hicks 2017). This is in line with the interpretation of Klein et al. (2017) about the sources of sediments.

The maximum sedimentation age is 2050 Ma, based on well-constrained detrital zircon U-Pb ages (Klein et al. 2017), whereas the minimum age is given by the intrusion of a dacite porphyry, which cut across the strata, at 2011 ± 6 Ma (Queiroz et al. 2015). Klein et al. (2017) interpreted the Castelo dos Sonhos Formation as part of a foreland system related to Rhyacian orogens of the Amazonian Craton (e.g., the Bacajá and Santana do Araguaia domains), and that sedimentation slightly preceded or was coeval with the onset of the orogenic phase in the Tapajós Gold Province (2.03-1.95 Ga).

4. Sampling and analytical procedures

Samples were obtained mostly from drill cores of the mineralized areas, in addition to surface exposures in old and recent artisanal mining pits. Location of the sampled drill cores and outcrops is shown in Figure 3A and presented in the Appendix A (electronic supplementary material). Information on the morphology of gold particles was obtained through conventional and scanning electronic microscopy (SEM). SEM analyses were done at the Laboratório de Microscopia Eletrônica de Varredura (LABMEV) of the Universidade Federal do Pará, in Belém, Brazil. Electronic microprobe chemical analyses of gold particles and white mica grains were performed at the Laboratório de Microssonda Eletrônica (LME) of the Universidade de Brasília, Brazil, using a JEOL JXA 8230 equipment. Concentrations of Au, Ag, W, As, Zn, Pb, Bi, Te, Cd, Co, Cu, Sb, Hg, Ni, Pd and Pt were obtained during Au analyses, and major elements (oxides) and Li, F, Cl and H_2O, during mica analyses. We used the following analytical conditions: acceleration voltage of 20 kV, current on the sample of 2.01 x 10-8 Å, counting time of 30 s per element. Oxygen isotopes in quartz and muscovite were analyzed at the Laboratório de Isótopos Estáveis da Universidade Federal de Pernambuco (LABISE-UFPE), in Recife, Brazil. Oxygen was liberated by reaction with BrF5 using a CO_2-laser, and then converted to CO2 by reaction with graphite at 75°C. The obtained CO_2 gas was isotopically analyzed in a Thermofinnigan Delta V Advantage mass spectrometer. Results are reported in the δ notation (‰) relative to the V-SMOW standard, with precision better than ± 0.1‰.

5. The Castelo de Sonhos gold deposit

5.1. Host rocks

In addition to what was presented in section 3, we describe below, in more detail, the metaconglomerates and metasandstones that host the gold mineralization, based on mesoscopic and microscopic petrographic studies performed in samples taken from drill cores of mineralized areas and from outcrops, mostly from the Esperança South, East and Center targets (Fig. 3A).

5.1.1. Metaconglomerates

The metaconglomerates are massive and range from fine- to very coarse-grained polymictic rocks composed of well-rounded to sub-angular, centimeter- to meter-thick clasts (Fig. 5). The clasts are predominantly quartz from veins and subordinately quartzite, banded iron formation, schists, tourmalinite and scarce metavolcanic rocks. Vargas and Campbell-Hicks (2017) also described the presence of pebbles and cobbles of the Castelo dos Sonhos Formation itself, which

suggests reworking of older lobes of the alluvial fan by younger lobes. The quartz-mica-clay matrix is strongly silicified, which is given by quartz cement, and shows reddish color, which was produced by local to pervasive impregnation of secondary iron oxides. In places, original textures and structures were obliterated by this iron oxide impregnation (Fig.5). Both clast- and matrix-supported varieties have been observed, but according to Appleyard et al. (2016), the clast-supported rocks appear to be less continuous and deposited in channels.

The primary sedimentary structures are in general well preserved, with bedding showing general NW-SE direction and variable dips, from 28 to 54° to SW. Locally, ductile deformation imparted a mylonitic foliation to the rocks (Fig. 6A and B), and late brittle deformation produced multidirectional fractures that cut across both clasts and matrix, and that are in general filled by magnetite and hematite (Fig. 7). Quartz veinlets containing rare pyrite and calcite are observed (Fig. 6C).

FIGURE 5 - Images of metaconglomerates of the Castelo de Sonhos deposit. (A) General view of an artisanal mining pit. (B) Closer view of the clast-supported metaconglomerate, with pebbles of variable shapes and sizes. (C) Drill cores showing, from left to right: impregnation of secondary iron oxides in the matrix and in fractures; clast-supported metaconglomerate; clast of banded iron formation; fractures coated by secondary iron oxides; strong impregnation of the matrix with secondary iron oxides; fracture coated by secondary iron oxides cutting across matrix and clasts.

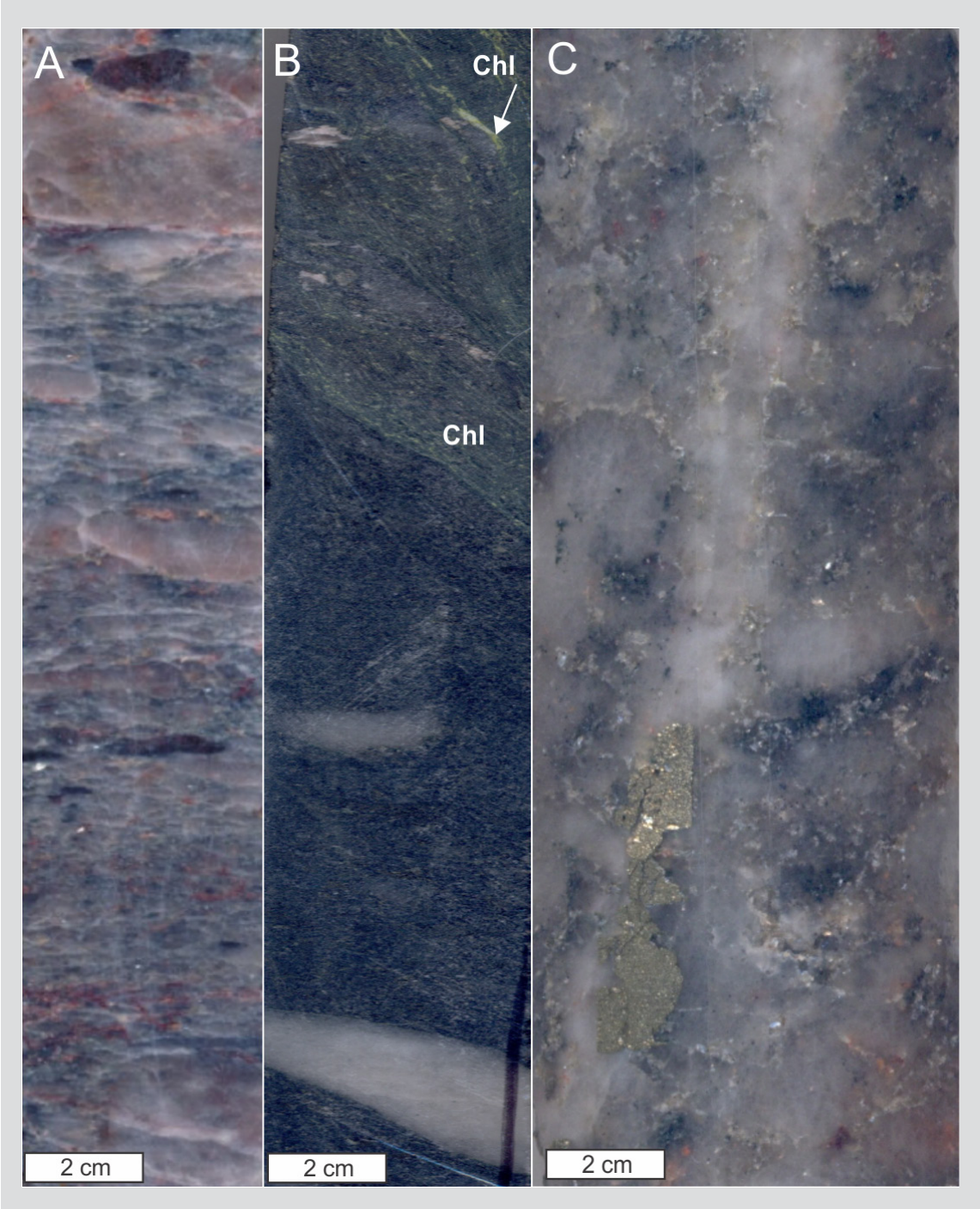

FIGURE 6 - (A) Deformed metaconglomerate showing orientation of matrix and elongation of clasts. (B) Mylonitic metaconglomerate with metamorphic/hydrothermal (?) chlorite (Chl). (C) Quartz-pyrite veinlet crosscutting metaconglomerate.

The medium- to coarse-grained matrix reveals to be composed mainly of quartz and white mica (Fig. 7A), in addition to magnetite, hematite, chlorite, tourmaline and zircon. Sulfide minerals (pyrite and chalcopyrite) are very rare and occur as idiomorphic intergranular grains. The more deformed portions of the rocks are characterized by matrix grain-size reduction (Fig. 7B) and the development of a heterogeneous mylonitic foliation defined by the orientation of white mica and chlorite and by stretching of grains and/or clasts of quartz. The quartz grains are, in general, monocrystalline, angular, with moderate to strong undulose extinction, and sutured or concave-convex contacts (Fig. 7A). These forms of contact indicate occurrence of pressure solution, which hinders the determination of the rounding degree and of the original limits between the grains. The white mica flakes are interstitial, occasionally associated with chlorite, and with random orientation. However, in more deformed and/or metamorphosed portions, the mica flakes are weakly to strongly oriented and coarser-grained (recrystallized), contorted or with strong undulose extinction (Fig. 7C and D). Magnetite is usually altered to hematite (Fig. 7E). A ferruginous cement fills both the primary and the secondary porosity of the rocks (Fig. 7F).

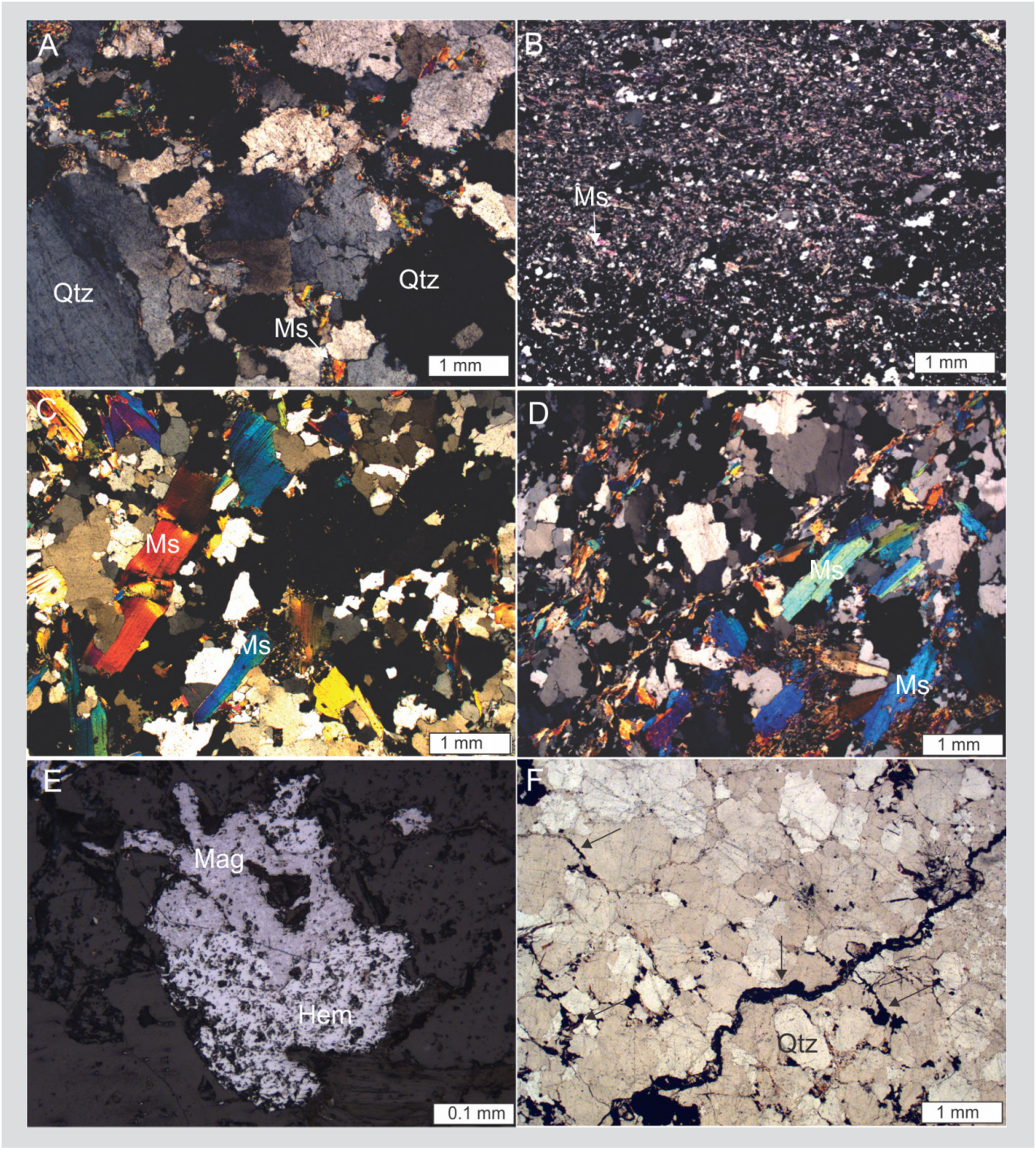

FIGURE 7 - Microscopic features of metaconglomerates. (A) Coarse-grained quartz-mica matrix with angular and subangular quartz grains showing concave-convex and sutured contacts. (B) Matrix with mylonitic foliation. (C) Coarse-grained, recrystallized white mica with undulose extinction. (D) Oriented crystals of white mica. (E) Hematite substitution of magnetite. (F) Ferruginous cement (arrows) filling primary and secondary porosity. Ms: muscovite (white mica), Qtz: quartz, Hem: hematite, Mag: magnetite.

5.1.2. Metasandstones

The metasandstones are massive, medium- to coarse-grained and poorly sorted, with occasional dispersed quartz granules. Just like the metaconglomerates, the metasandstones are also strongly silicified, with pervasive impregnation of secondary iron oxides, which also occur filling fractures (Fig. 8). In addition, the widespread preservation of the sedimentary structures, and the same structural features present in the metaconglomerates are observed in the metasandstones (Fig. 8B). However, quartz veinlets (Fig. 8C) are rare.

Compositionally, the protoliths of the metasandstones are quartz-arenites (Folk 1974). The mineralogical composition is identical to that of the matrix of the metaconglomerates, i.e., quartz (95%), white mica, magnetite, hematite, chlorite, tourmaline and zircon, along with rare pyrite and chalcopyrite. Individual grains of quartz exhibit moderate to strong undulose

extinction and are strongly fractured. The grains are poorly rounded, with sutured and concave-convex contacts(Fig. 9A), showing micro-stylolite (Fig. 9B). White mica forms small interstitial flakes (Fig. 9C). Ferruginous cement fills the primary and secondary porosity of the rocks (Fig. 9D and E). In the deformed portions of the metasandstones, the mylonitic foliation is defined by oriented lamellae of white mica and stretching of quartz grains (Fig. 9F). Magnetite is variably (weakly to strongly) replaced by hematite (Fig. 9G), which also occur as individual grains (complete substitution of magnetite?), locally associated with pyrite (Fig. 9H).

5.2. Gold mineralization

The metaconglomerates of the central metaconglomerate layer (Unit II, in Fig. 4B) are the main hosts of the mineralization, and there is a clear relationship between the areas of metaconglomerate outcrops and gold anomalies in soil (Mello 2014). According to Vargas and Campbell-Hicks (2017), the strike length of the mineralized metaconglomerate is about 16 km. The individual mineralized reefs range from 1 m to 20 m in thickness, and strike north-south, with dips of 20° to 30° to the west. Partial resources have been reported for the upper 120 m

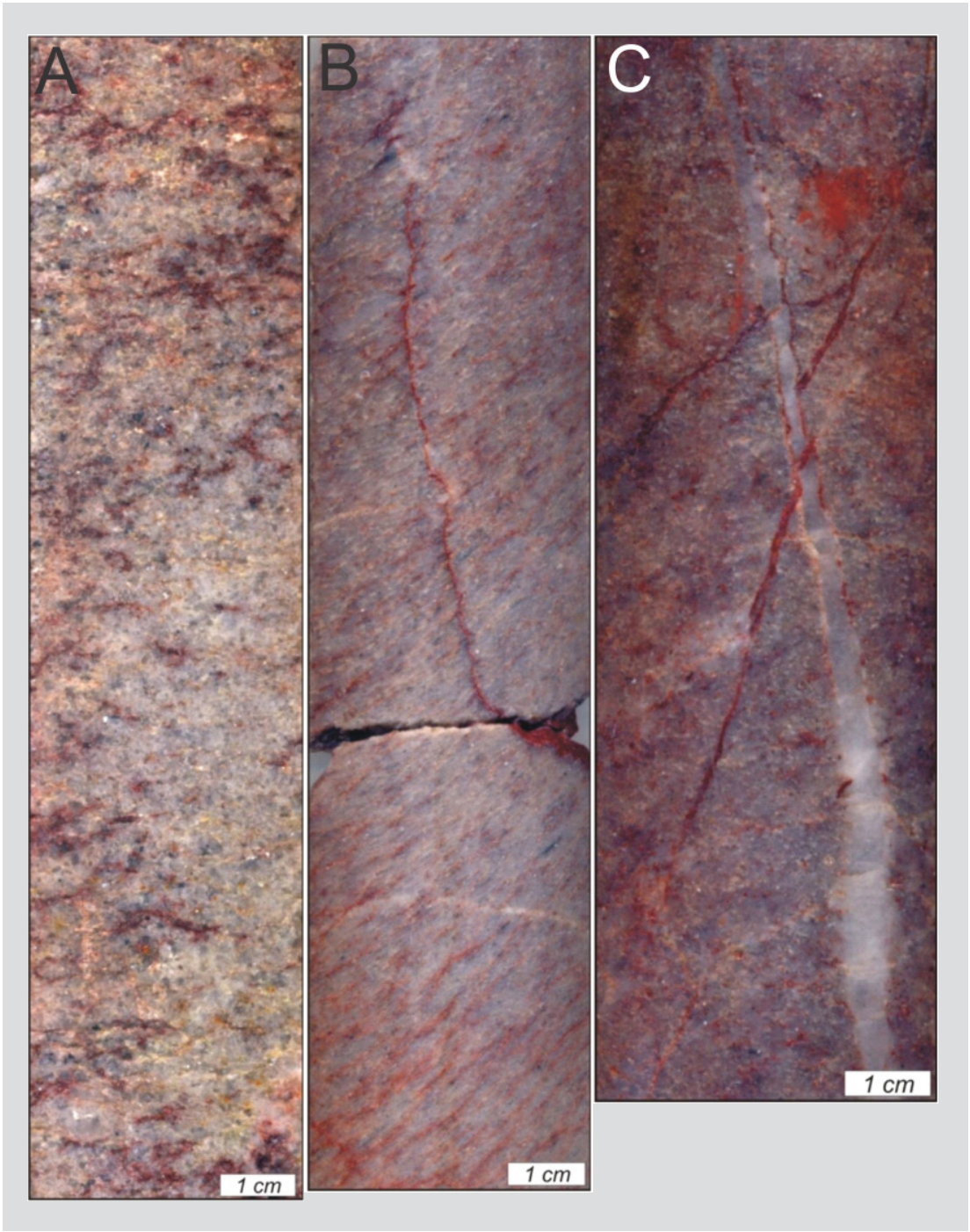

FIGURE 8 - Mesoscopic aspects of metasandstones. (A) Medium-grained, massive metasandstone, with local impregnation of secondary iron oxides. (B) Deformed (mylonitic) metasandstone with impregnation of secondary iron oxides. (C) Quartz veinlet cutting across mylonitic metasandstone.

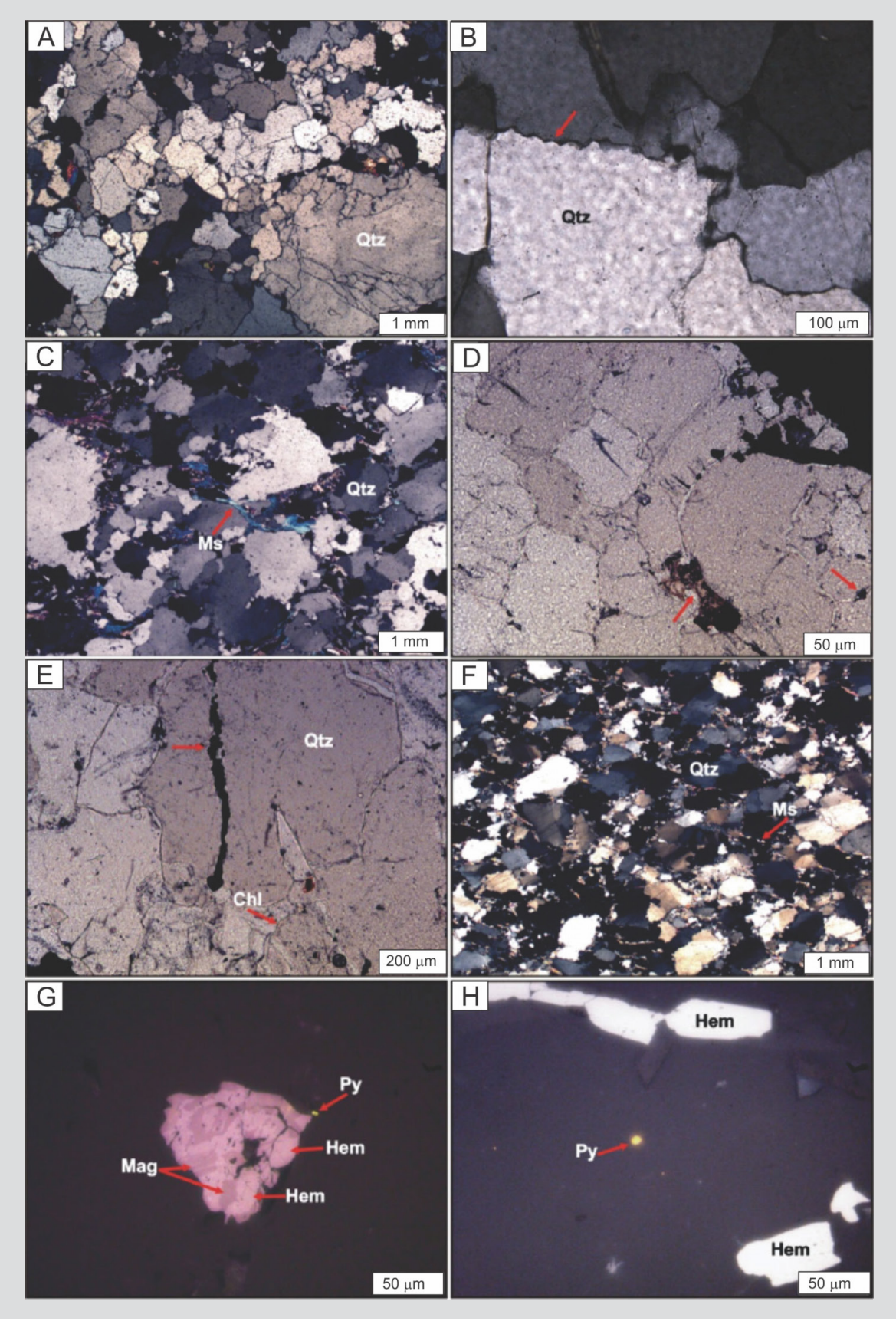

FIGURE 9 - Microscopic aspects of metasandstones. (A) Angular to subangular quartz grains exhibiting concave-convex and sutured contacts. (B) Stylolite contact (arrow). (C) White mica flakes contorted and "smashed" between quartz grains. (D) Ferruginous cement filling primary pore (arrow). (E) Ferruginous cement filling secondary porosity (arrow) in a chlorite-bearing sandstone. (F) Foliation in metasandstone. (G) Magnetite partially replaced by hematite, in contact with small pyrite crystal. (H) Small pyrite crystal within quartz grain, in spatial association with hematite. Qtz: quartz, Ms: muscovite (white mica), Chl: chlorite, Mag: magnetite, Hem: hematite, Py: pyrite.

of the deposit, although mineralization has been detected down to 300 m. Within the mineralized beds, gold grades are very variable and, in average, the Esperança Center target shows higher grades. Furthermore, depending on the adopted cut-off, the thickness of the mineralized layers may exceed 50 m. Vargas and Campbell-Hicks (2017) also described the presence of gold in heavy mineral bands, which, in addition to the random distribution of gold grades associated with the metaconglomerate layers indicate absence of structural control and deposition of gold along with the sediments. Even in high-grade intersections, it is not possible to distinguish mineralized from barren rocks, except when visible gold is present. In general, strong silicification and widespread iron oxides impregnation have been used as an exploration guide and interpreted as hydrothermal alteration, i.e., silicification and hematite alteration (Mello 2014; Appleyard et al. 2016), although the processes affect also barren rocks.

Gold is present in the matrix of the metaconglomerates and we have observed three different forms of occurrence (Fig. 10): (1) within detrital quartz grains, (2) as intergranular particles, frequently in contact with white mica, and (3) spatially associated to magnetite.

In the metasandstones, gold occurs in the matrix, similarly to what is observed in metaconglomerates. Vargas and Campbell-Hicks (2017) interpret this mineralization as product of remobilization induced by hydrothermal. However, no evidence has been presented to confirm this.

A second and subordinate type of mineralization is defined by the presence of gold in small fractures coated with secondary iron oxides (Fig. 11), cutting across metasandstones. Although we have not found gold in fractures that cut across the metaconglomerates, this feature has been observed during the exploration work (Vargas and Campbell-Hicks 2017).

It is worth of noting that carbonaceous matter, detrital pyrite and U-bearing minerals have not been observed neither in metasandstones nor in metaconglomerates.

5.2.1. Morphology of the gold particles

Representative samples from the two styles of mineralization (matrix of the metaconglomerates and fractures in metasandstones) have been used for morphological characterization of gold particles. Particles found in the matrix of the metaconglomerate (Fig. 12) are 7 to 200 μm long and exhibit various shapes, mainly rectangular, spheroidal (equant), ellipsoidal (blunted), and irregular, with rounded to subrounded rims and weakly to strongly rugged surfaces. Few are spongy. Occasionally, the gold grains occur in association with magnetite. Some particles exhibit cavities and saliences, solid inclusions are rare and consist always of magnetite. Few particles show relic crystalline forms.

Gold particles recovered from fractures in the metasandstone (Fig. 13) are larger (180-500 μm) than those found in the metaconglomerates. These particles are rather fragile, very thin (flattened), with subrounded to angular rims and rugged surfaces, and coated with secondary iron oxides. Slightly curved particles have also been observed.

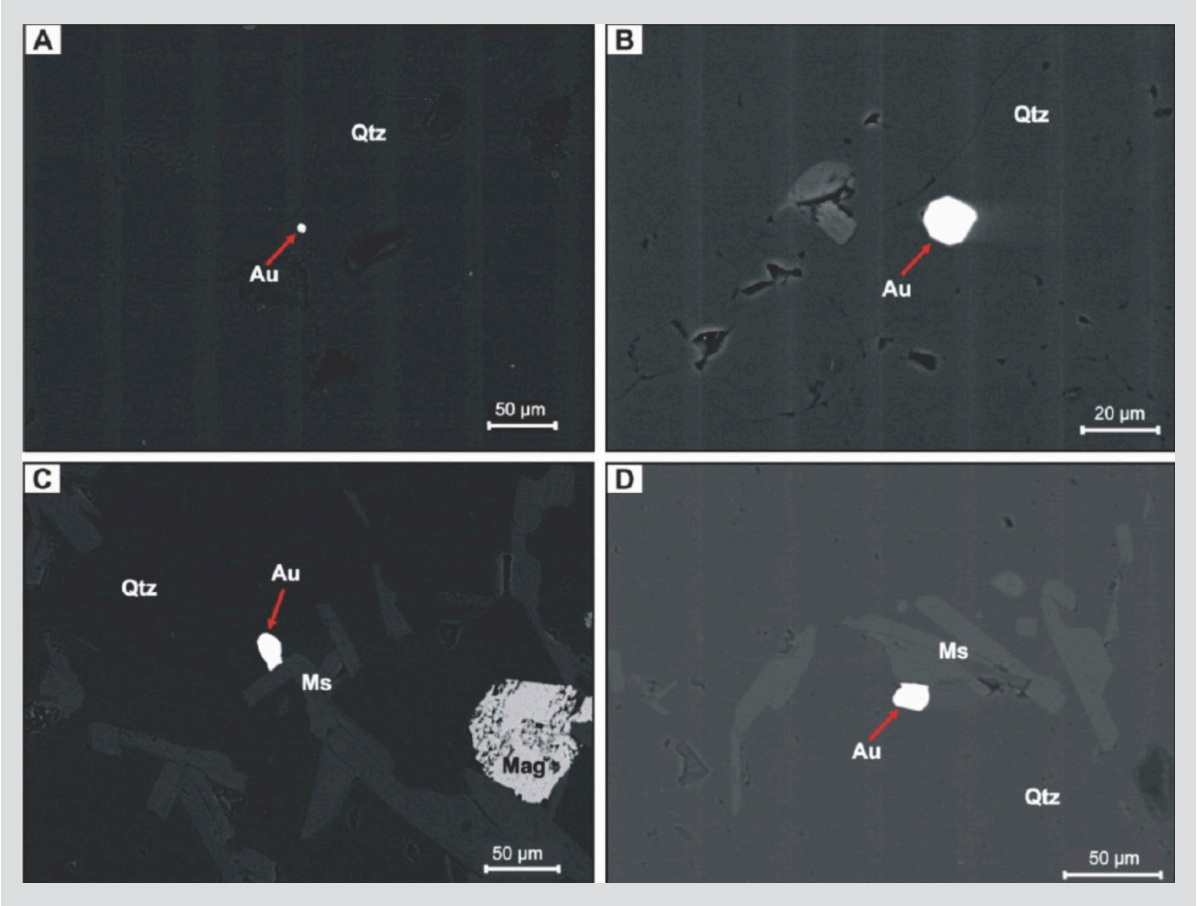

FIGURE 10 - Backscattered electron images of gold in the matrix of metaconglomerate (thin sections). (A) and (B) Gold in the inner portions of detrital quartz grains. (C) and (D) Intergranular particles in contact with muscovite. Qtz: quartz, Ms: muscovite (white mica).

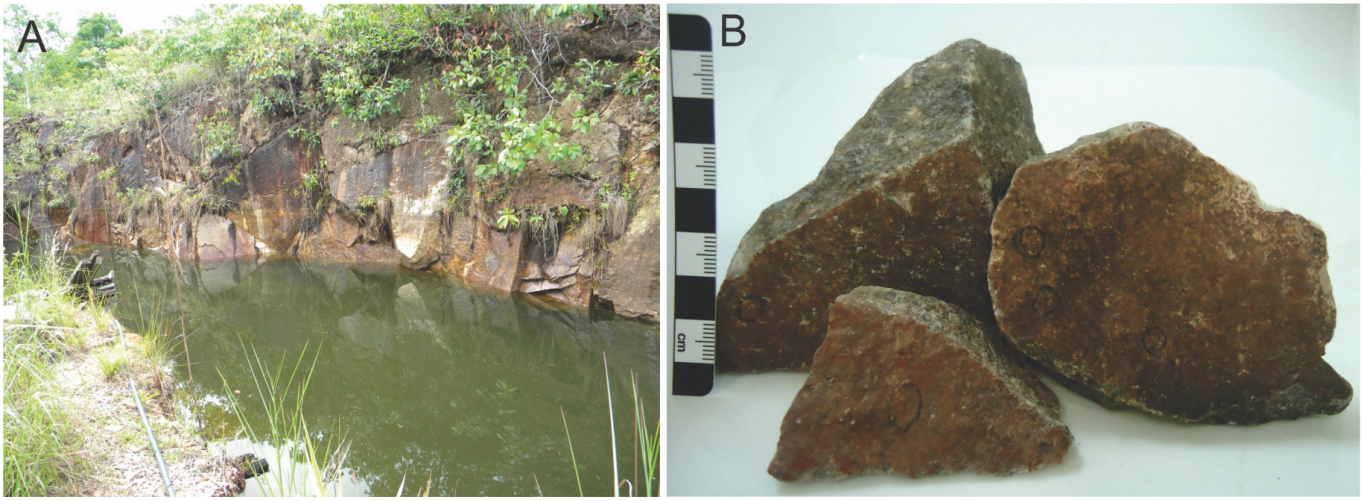

FIGURE 11 - (A) General view of an old open-pit in metasandstone. (B) Hand samples of metasandstone with gold particles (within circles) hosted in fractures coated with secondary iron oxides.

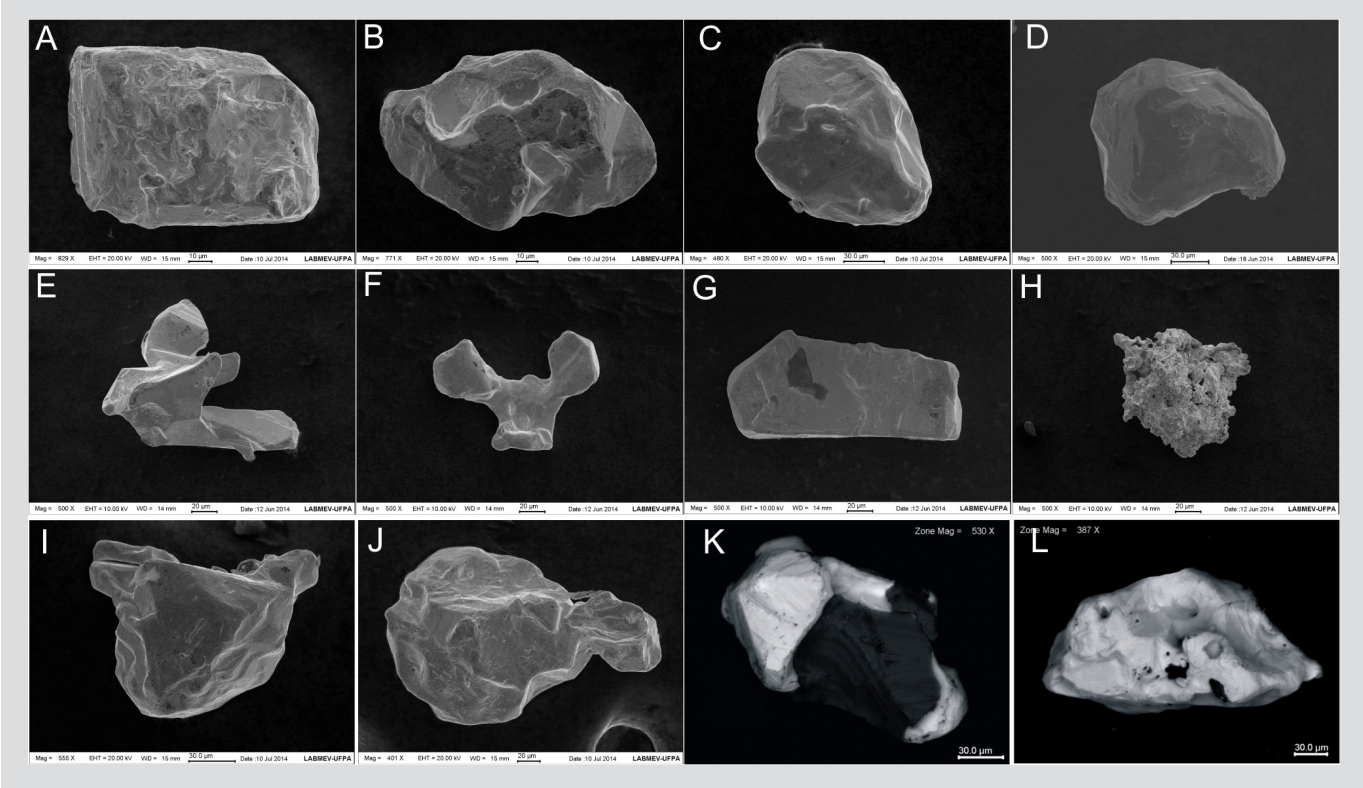

FIGURE 12 - Backscattered electron images of individual gold particles from the matrix of metaconglomerate showing the variation in morphology. (A) and (B) Rectangular to ellipsoidal with rounded to subrounded terminations. (C) and (D) Equant, rounded or blunted. (E) and (F) Irregular. (G) Elongated. (A to G have smooth surfaces). (H) Spongy. (I) and (J) Irregular with rounded to subrounded terminations and rather rugose surface. (K) Gold in contact with magnetite. Note the relict shape of the particle. (L) Irregular particle with cavities and inclusion of magnetite.

5.2.2. Mineral chemistry of gold

The chemical composition of gold particles from the two types of mineralization, measured by electronic microprobe, is presented in Appendix B (electronic supplementary material). The composition is quite homogeneous for the two types, with gold grading 94 to 99%, and silver contents ranging from <1 to 4.7% (Fig. 14), which gives very high Au/Ag ratios. Results obtained in core and rim of the gold particles do not show significant difference. The only noteworthy difference regards the silver contents of the particles sampled in fractures, which are very low (<<1%, Appendix B and Fig. 14), given even higher Au/Ag ratios than those observed in gold particles from the matrix of the metaconglomerates.

All other analyzed elements, when present, occur only in trace amounts (<1%). Although always below 1%, mercury is the element with the highest grades and was detected in most of the particles from both metaconglomerate and metasandstone (0.03 to 0.73% and 0.09 to 0.52%, respectively, Fig. 14). Palladium, Te, Sb and Cd also occur in most of the gold grains, Ni, Co and Pt were frequently detected, whereas Zn, Pb, Cu are seldom present.

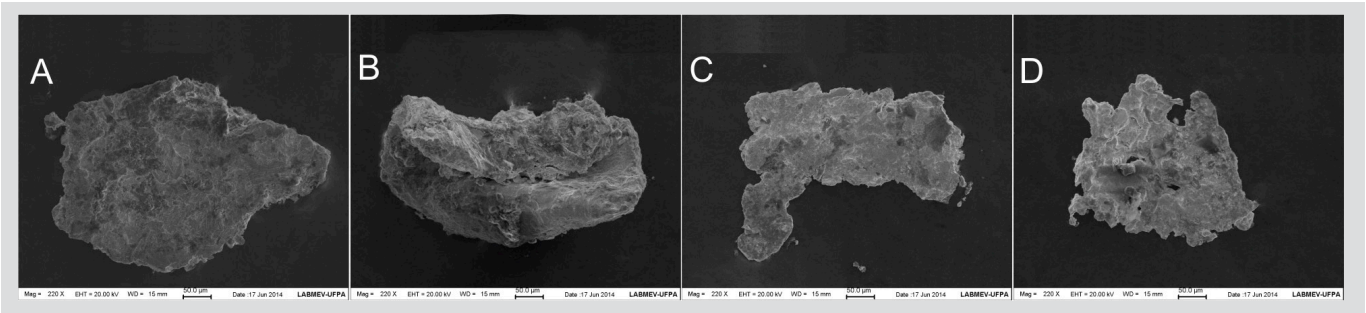

FIGURE 13 - Backscattered electron images of individual gold particles hosted in fractures of metasandstone. All particles are flattened, with irregular edges and rugose surface.

5.3. Mineral chemistry of white mica

A reconnaissance study was performed in white mica grains from the matrix of a metaconglomerate (CM), sampled at different depths, and from a coarse-grained quartz-mica vein (VM) that cut across a metasandstone. The results are presented in Appendix C (electronic supplementary material).

The CM show relatively homogeneous composition, except for the deepest sample, which shows nevertheless only slightly different composition, defined by lower Al_2O_3 and octahedral Al, and the highest TiO_2 and MgO contents among all analyzed samples. The composition VM is not very different from that of CM. However, VM shows the highest Mn, Li, F and tetrahedral Al, and the lowest Si and Ba contents among the studied samples. In fact, the CM lack Li and F, except for the deepest sample.

All analyzed samples belong to the muscovite end member, according to the classifications of Monier and Robert (1986 – Fig. 15A) and of Tischendorf et al. (1997 –figure not included). A biotite substitution trend is also defined by the composition (Fig. 15B). According to Miller et al. (1981), CM are secondary in origin, with the exception of the deepest sample, which falls, together with VM, in the field of primary muscovite (Fig. 16).

5.4. Oxygen isotopes

The stable isotope composition of oxygen were determined in quartz from veinlets, and from the coarse-grained quartz-muscovite vein (same VM as above) that cut across the metasedimentary host rocks and one tonalite that intruded into the metasedimentary sequence. The results are shown in Table 1).

The $\delta^{18}O$ values of quartz from veinlets range from 10.9 to 16.8 ‰, which indicate variable crystallization temperature and/or fluid composition. Quartz and muscovite from VM show $\delta^{18}O$ values of 10.9 and 9.3 ‰, respectively. Assuming equilibrium, this quartz-muscovite pair yields a formation temperature of 673°C (Chacko et al. 1996), whereas the fluid in equilibrium with the minerals has a $\delta^{18}O$ value of 10.5 ‰ (Matsuhisa et al. 1979). This value most likely reflects magmatic origin (Sheppard 1986). If a similar temperature is assumed for the other samples, higher $\delta^{18}O_{H2O}$ values are obtained (10.5 to 16.3 ‰), still compatible with a magmatic origin and with no evidence of meteoric contribution.

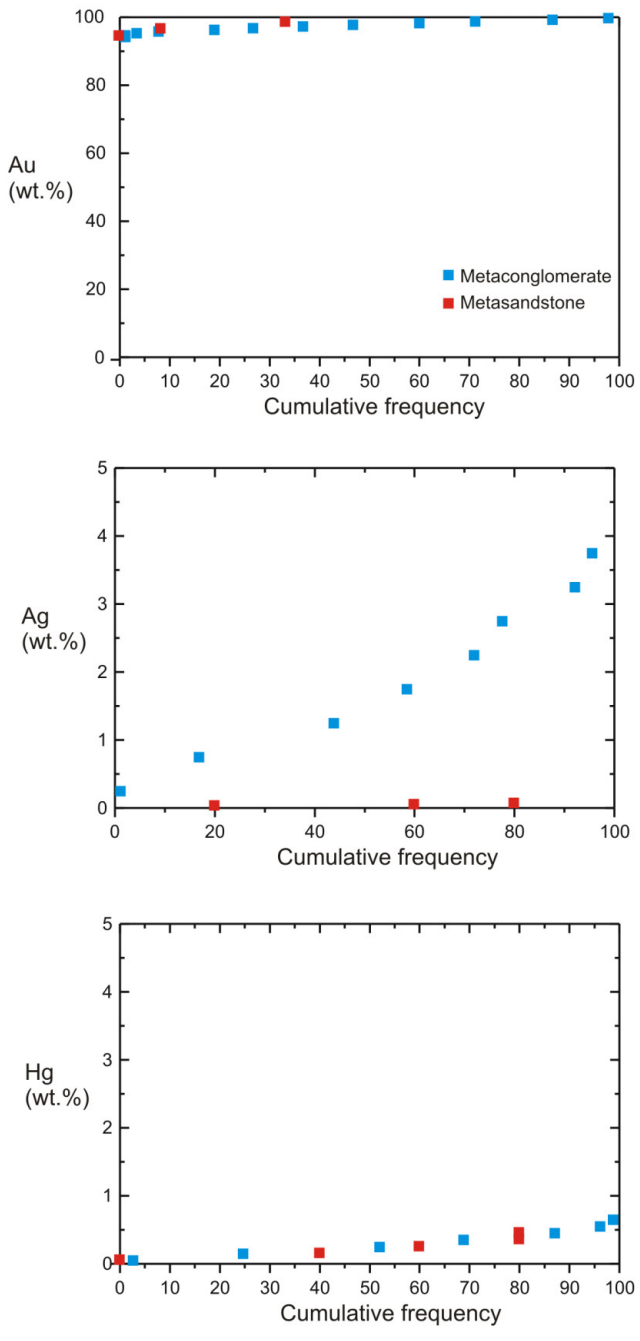

FIGURE 14 - Cumulative frequency diagrams of Au, Ag and Hg compositions in gold partivles from metaconglomerate and metasandstone.

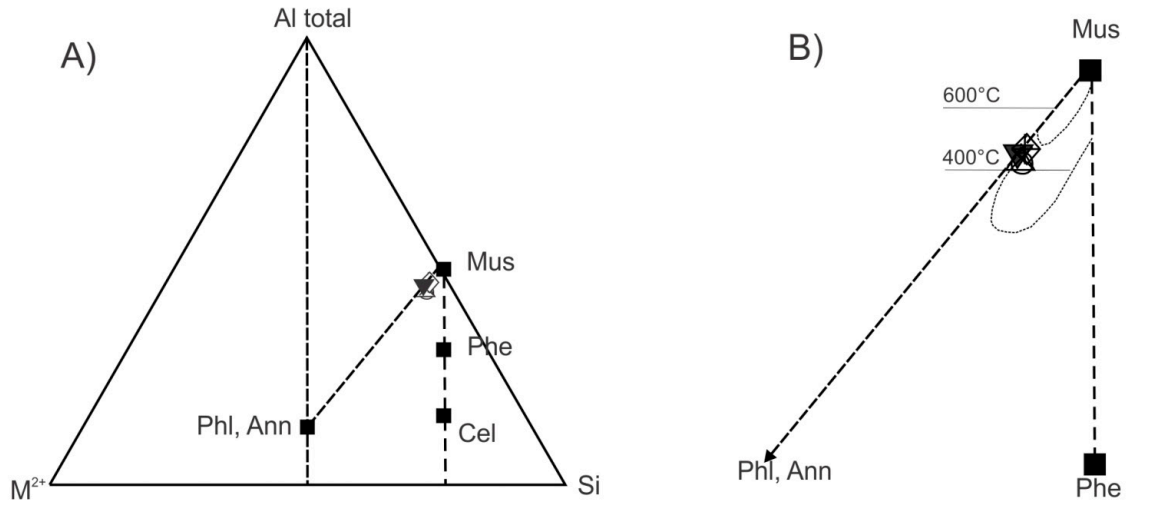

FIGURE 15 - (A) Diagram Total Al-M^{2+}-Si (atomic proportions) of Monier and Robert (1986) for white mica grains of the Castelo de Sonhos gold deposit (data from Appendix C), where M^{2+} corresponds to divalent Fe and Mg. (B) Detail of the same diagram indicating biotite substitution trend. Phl: phlogopite, Ann: annite, Cel: celadonite, Phe: phengite, Mus: muscovite. Open symbols (CM), filled triangle (VM).

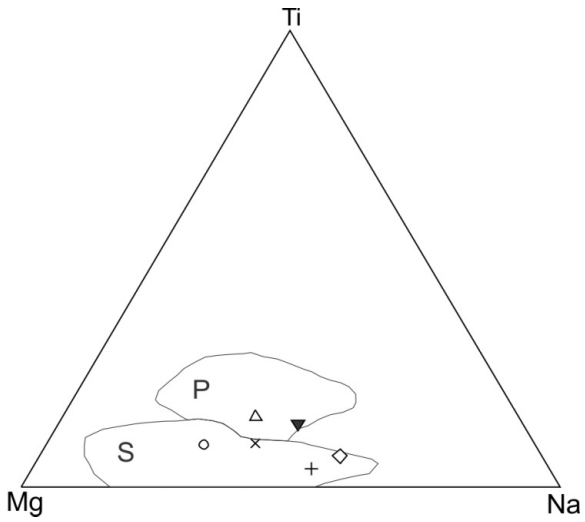

FIGURE 16 - Diagram Mg-Ti-Na (atomic proportions) from Miller et al. (1981) for white mica grains of the Castelo de Sonhos gold deposit (data from Appendix C), with the fields of primary (P) and secondary (S) muscovite. Open symbols (CM), filled triangle (VM).

Table 1 - Stable oxygen isotope results for samples of the Castelo de Sonhos gold deposit

Sample*	Mineral	Style	Host rock	Δ18O (‰ V-SMOW)
01/231.30-232.00	Quartz	QV	metasandstone	15.3
44/32.05-32.20	Quartz	QV	metasandstone	10.9
31/7540-75.90	Quartz	QV	metaconglomerate	16.8
48/117.1-117.65	Quartz	QSCV	metaconglomerate	11.5
02/423.35-423.55	Quartz	QV	hb-bt tonalite	11.2
32/142.50-142.80	Muscovite	MV	metasandstone	9.3
32/142.50-142.80	Quartz	MV	metasandstone	10.9

*drill hole number/depth in meters
Abbreviations: QV: quartz vein, QSCV: quartz-sulfide-carbonate vein, MV: coarse-grained quartz-muscovite vein, hb: hornblende, bt: biotite

6. Discussions

6.1. Silicification and iron oxide impregnation: hydrothermal x diagenetic

The strong hardness (massive aspect) observed in the metaconglomerates and metasandstones, and the ubiquitous impregnations with secondary iron oxides have been attributed to hydrothermal silicification and hematite alteration (Mello 2014; Appleyard et al. 2016), respectively. However, as we show in this study, other processes have likely been involved in the silicification and iron oxide impregnation.

The iron oxide impregnation is only in part related to hydrothermal overprint. Significant part of the impregnation pervasively overprinted the rocks through precipitation of iron oxides-hydroxides on detrital grains (Figs. 5 and 8), and this is a diagenetic process quite common in continental sandstones (e.g., De Ros and Moraes 1984), which is the case of Castelo dos Sonhos Formation. Accordingly, the eodiagenetic modification of the detrital grains can liberate Fe^{+3} and Fe^{+2} ions and, depending on the pH and Eh conditions, the Fe^{+2} ion is maintained in solution, or is incorporated by authigenic phases, such as pyrite and smectite. The weakly soluble Fe^{+3} ion precipitates as iron oxide-hydroxide phases and, along with secondary oxidation of the observed Fe-bearing minerals (chlorite, pyrite, magnetite), impart the characteristic reddish-brown color to the rocks (Walker 1967, 1974; De Ros and Moraes 1984; Boggs Jr 2009). Late, post-diagenetic hydrothermal (magmatic, meteoric?) fluids might have remobilized iron that migrated through the network of fractures (Figs. 5 and 8).

Regarding silicification, small and discontinuous quartz veinlets and rare quartz-sulfide veinlets have been observed cutting across the hosting metasedimentary rocks (Figs. 6C and 8C), but this epigenetic veining process has no relationship with the widespread silicification. In the matrix of the metaconglomerates and metasandstones, the detrital quartz grains are typically affected by pressure solution, resulting in the development of concave-convex and sutured contacts (Figs. 7A and 9A), and in the transference of the soluble silica from lower- to higher pressure zones, cementing both the primary and secondary pores. This diagenetic to metamorphic silica overgrowth in the borders of detrital quartz grains strongly reduces the primary porosity and hardens the rocks (De Ros and Moraes 1984; Passchier and Trouw 2005).

6.2. Detrital gold (paleoplacer mineralization)

The main gold mineralization in the Castelo de Sonhos deposit is confined to a 300-400 m thick package of metaconglomerates and subordinate interbedded metasandstones deposited between 2050 and 2011 Ma. The random distribution of gold grades associated with the metaconglomerate layers indicates absence of structural control, which, in fact, has not been observed or reported so far. Gold is found in the matrix of the metaconglomerate, in spatial association with detrital magnetite, secondary muscovite, and also within detrital quartz grains (fragments of auriferous veins). Sulfides are very rare in the matrix of the metaconglomerates and, even when present, no association with gold particles has been observed. In addition, U-bearing minerals have not been observed. It is possible, however, that if sulfides were originally present as detrital grains, and they have been obliterated by subsequent oxidizing solutions. Gold particles are rounded to subrounded, with rugose surface, and only locally contain inclusions of magnetite. Rare veinlets of quartz-calcite-sulfide that crosscut metaconglomerates do not have gold, and no occurrence of gold in the contact zone between intrusive rocks and metaconglomerates have been reported to date. All these characteristics suggest that the gold particles have been mechanically transported together with other heavy minerals and that they have been abraded during sedimentary transportation. As a whole, the grains are not pristine and show modified and reshaped morphology and textural characteristics (Dilabio 1991). Nevertheless, the textures and detrital morphologies indicate relatively proximal distance of transport from the source(s).

Considering the low hardness of gold, its original morphology is easily modified by distance and mode of transportation. In addition, the abundance of solid inclusions tends to diminish in response to the physical disintegration and also by surficial post-depositional processes (McClenaghan 2009), and post-depositional chemical abrasion may also result in fragile and spongy textures. Therefore, this main mineralization is interpreted to be of detrital, paleoplacer origin.

6.2.1 Source of the detrital gold

The variation in the composition of gold is a consequence of differences in the geological setting, deposit class, and chemistry of ore-forming processes (e.g., Chapman et al. 2011). The homogeneous chemical composition of the detrital gold present in the matrix of the metaconglomerate, including the narrow range of silver contents, indicates a single source, or sourcing from a single deposit class (e.g., Craw et al. 2017), although multiple sources could be expected for a paleoplacer deposit, considering that the provenance study (Klein et al. 2017) showed multiple sources for detrital zircon of the hosting metaconglomerate. The high Au/Ag ratios and absence of significant content of any other metal suggest that the gold particles might have come from orogenic gold source(s) (Minter 1991). Au-Ag-Hg-Cu relationships (Fig. 17) are not completely clear about potential sources, although favor an orogenic source. Since all known magmatic-hydrothermal deposits from Tapajós are younger than Castelo de Sonhos, the sources of detrital gold must be external to the Tapajós Province, and are likely similar to those defined for the detrital zircons by Klein et al. (2017), i.e., Rhyacian orogenic belts and Archean basement located to the east, northeast and southeast of Tapajós. In fact, potential source deposits are widespread in these terranes (Klein et al. 2014; Monteiro et al. 2014). Notwithstanding, a word of caution must be stated, since gold samples from more targets within the deposit should be investigated to corroborate this assumption.

6.3. Epigenetic mineralization

Gold particles have been found filling fractures (Fig. 11) and filling the foliation of metasandstones (Mello 2014). The particles from fractures have Au/Ag ratios higher than those found in the matrix of the metaconglomerates. The mineralized fractures are coated with secondary iron oxides, but no timing relationship between gold deposition and iron oxide impregnation could be established.

The gold present in fractures has been attributed to supergene remobilization of the gold present in metaconglomerates (Mello 2014). However, we understand that epigenetic/hydrothermal remobilization is a more likely process. Parallel to the diagenesis stages, deformation plays important role favoring fluid movement and inducing local and regional gradients in the hydraulic potential. In the process, the following effects are common: (1) increase in the fluid pressure related to compression, which usually occurs in depth, in association with ductile deformation and metamorphism, leading to mineral dehydration reactions; and (2) decrease in the fluid pressure in shallower depths, induced by space opening by fracturing (Sibson 1994; Oliver 1996; Cox 2005; Zhang et al. 2008). The resulting gradient in the hydraulic potential provides the necessary energy for fluid ascent in the crust, and this fluid may be channelized to dilation zones related to shallow brittle deformation, according to the pump-suction model of Sibson (1994).

Regarding to the Castelo de Sonhos deposit, it is likely that the interaction of the above described sedimentary, metamorphic, magmatic and deformation processes have contributed to the production and circulation of oxidizing hydrothermal fluids, which were capable of the solubilization of gold and iron from the matrix of the metaconglomerates and deposition of these elements in fractures in neighboring rocks (remobilization). The higher fineness (higher Au/Ag ratios) might be explained by: (1) the higher solubility of silver when compared to that of gold in surface and oxidizing conditions (Boyle 1979; Webster and Mann 1984); (2) gold transport by chloride oxidizing systems, with silver being present as a solid Ag chloride, such as chlorargyrite, and is not available for transport in solution (Chapman et al. 2009).

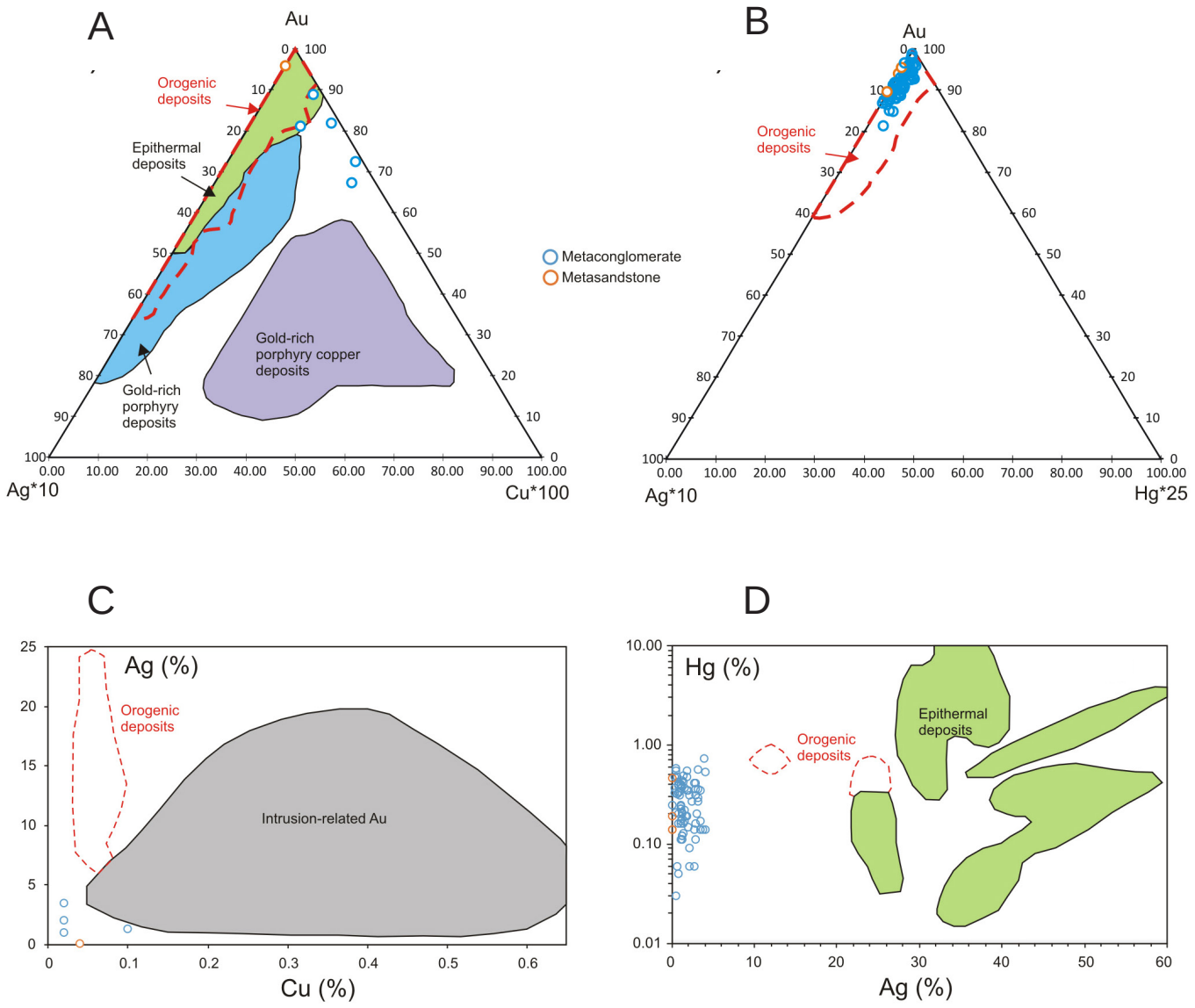

FIGURA 17 - Chemical composition of gold particles of the Castelo de Sonhos gold deposit compared to potential sources. (A) Au – Ag*10 – Cu*100; fields for epithermal, Au-rich porphyry and Au-rich porphyry copper deposits are from Townley et al. (2003), and for orogenic deposits are from Omang et al. 2015. (B) Au – Ag*10 – Hg*25; field for orogenic deposits from Omang et al. (2015). (C) Cu – Ag; fields for intrusion-related and orogenic gold are from Chapman et al. (2011). (D) Ag – Hg; fields for epithermal and orogenic gold from Chapman et al. (2011).

7. Conclusions

Considering (1) the characteristics of the two styles of mineralization, i.e., deposited in the matrix of metaconglomerates and in fractures, (2) that the Castelo dos Sonhos Formation was deposited in a relatively short time (2050-2011 Ma), (3) and then was intruded by different generations of granitoids (4) and underwent deformation and low-grade metamorphism (timing unknown), we suggested a hybrid syngenetic-epigenetic (modified paleoplacer) model for the gold deposit. The uniform and minor and trace-element poor chemical composition of the detrital gold particles suggest that they were sourced from a single source or, more probably, single class of deposit (orogenic gold), whereas the age of gold deposition (2011-2050 Ma) indicate sources external to the younger Tapajós Gold Province. On petrographic grounds, the observed silicification of the metaconglomerates and metasandstones is a diagenetic process, not related to hydrothermal alteration. Accordingly, after the sedimentation associated with deposition of detrital gold (main mineralization), the interaction between sedimentary, metamorphic and magmatic processes and deformation contributed to the production and circulation of oxidizing hydrothermal fluids, which percolated the gold-bearing metaconglomerates and were able to solubilize part of the detrital gold. Based on stable isotope compositions of quartz and muscovite, the fluids are of magmatic origin, and we speculate that these were derived from granites that intruded the Castelo dos Sonhos basin. The brittle deformation played a key role in generating the fractures that focused the gold-bearing fluids. Possibly, the infiltration of fluids led to the reprecipitation of solubilized gold, accompanied by secondary iron oxide films, in fractures of the metasandstones.

Acknowledgements

The authors are indebted to Elton Pereira and Fabio Mozer from TriStar Gold Inc. for allowing access to the Castelo de Sonhos project. JDSQ thanks Coordenação de Aperfeiçoamento de Pessoal de Nível Superior (CAPES) for a scholarship and ELK thanks Conselho Nacional de Desenvolvimento Científico e Tecnológico (CNPq) for research grant (306798/2016-6). The paper is a contribution to the GEOCIAM (Instituto Nacional de Ciência e Tecnologia da Amazônia) project. Reviews of Robert Chapman, Eric Lipten, and Wilson Scarpelli allowed a significant improvement of the manuscript and were greatly appreciated.

References

Alkmin F.F. 2011. Stratigraphy and structure of the Castelo dos Sonhos gold mineralization host rocks, southern Pará: Brazil. Unpubl. internal report, Tristar Gold, 15 p.

Appleyard N., Brown A., Srivastava M. 2016. Exploration Target Range for the Castelo de Sonhos Gold Project Pará State – Brazil. National Instrument 43-101 Technical Report, Tristar Gold, 52 p. Available online at: https://www.sedar.com/GetFile.do?lang=EN&docClass=24&issuerNo=00030238&issuerType=03&projectNo=02452359&docId=3875449 / (accessed on 3 July 2018)

Boggs Jr. S. 2009. Petrology of Sedimentary Rocks. New York, USA: Cambridge University Press, 2ed., 600 p.

Boyle R.W. 1979. The geochemistry of gold and its deposits, Geological Survey of Canada, Bulletin 280, 584 p.

Chacko T., Hu X., Mayeda T.K., Clayton R.N., Goldsmith J.R. 1996. Oxygen isotope fractionations in muscovite, phlogopite, and rutile. Geochimica et Cosmochimica Acta, 60, 2595-2608.

Chapman R.J., Leake R.C., Bond D.P.G., Stedra V., Fairgrieve B. 2009. Chemical and Mineralogical Signatures of Gold Formed in Oxidizing Chloride Hydrothermal Systems and their Significance within Populations of Placer Gold Grains Collected during Reconnaissance. Economic Geology, 104, 563-585.

Chapman R.J., Mortensen J.K., LeBarge W.P. 2011. Styles of lode gold mineralization contributing to the placers of the Indian River and Black Hills Creek, Yukon Territory, Canada as deduced from microchemical characterization of placer gold grains. Mineralium Deposita, 46, 881-903. https://doi.org/10.1007/s00126-011-0356-5

Cox S.F. 2005. Coupling between deformation, fluid pressures, and fluid flow in ore producing hydrothermal systems at depth in the crust. In: Hedenquist J.W., Thompson J.F.H., Goldfarb R.J., Richards J.P. (Eds.), Economic Geology One Hundredth Anniversary Volume. Society of Economic Geologists, 39-76.

Craw D., McLachlan C., Negrini M., Becker N. 2017. Quantification and Prediction of Bulk Gold Fineness at Placer Gold Mines: A New Zealand Example. Minerals, 7, 226. http://doi.org/10.3390/min7110226

De Ros L.F., Moraes M.A.S. 1984. Sequência diagenética em arenitos: uma discussão inicial. In: Congresso Brasileiro de Geologia, 33, Rio de Janeiro, Sociedade Brasileira de Geologia, Anais... p. 894-904.

Dilabio R.N.W. 1991. Classification and interpretation of the shapes and surface textures of gold grains from till. In: Hérail G., Fornari M. (eds.) Gisements alluviaux d'or. Symposium International sur les Gisements Alluviaux d'Or, La Paz, Bolívia, 297-313.

Folk R. L. 1974. Petrology of Sedimentary Rocks. Hemphill Publishing Co. Austin, Texas 184 p.

Frimmel H.E. 2014. A giant Mesoarchean crustal gold-enrichment episode: Possible causes and consequences for exploration. Society of Economic Geology Special Publication 18, 209-234.

Guimarães S.B., Klein E.L., Chaves C.L., Castro J.M.R., Souza-Gaia S.M., Queiroz J.D.S., Feio J.V.B., Lima R.G.C. 2015. Geologia e recursos minerais do sudeste do Tapajós. Informe de Recursos Minerais, Série Províncias Minerais do Brasil, 3, 61 p, Available at: <http://rigeo.cprm.gov.br/jspui/handle/doc/16601>

Juliani C., Fernandes C.M.D., Monteiro L.V.S. 2015. Características da subducção, paleoclima e eventos erosivos paleoproterozoicos (2,1-1,88 Ga) e seus efeitos na estruturação da parte sul do Cráton Amazônico. In: Simpósio de Geologia da Amazônia, Sociedade Brasileira de Geologia-NO, Annals (CD-ROM), 13 p.

Klein E.L., Almeida M.E., Rosa-Costa L.T. 2012. The 1.89-1.87 Ga Uatumã Silicic Large Igneous Province, northern South America: Large Igneous Provinces Commission. <http://www.largeigneousprovinces.org>.

Klein E.L., Rosa-Costa L.T., Vasquez M.L. 2014. Metalogênese da borda oriental do Cráton Amazônico. In: Silva M.G., Rocha Neto M.B., Jost H., Kuyumjian R.M. (eds), Metalogênese das Províncias Tectônicas Brasileiras. Belo Horizonte, CPRM, p. 171-194.

Klein E.L., Rodrigues J.B., Queiroz J.D.S., Oliveira R.G., Guimarães S.B., Chaves C.L. 2017. Deposition and tectonic setting of the Palaeoproterozoic Castelo dos Sonhos metasedimentary formation, Tapajós Gold Province, Amazonian Craton, Brazil: age and isotopic constraints. International Geology Review, 59, 864-883. http://dx.doi.org/10.1080/00206814.2016.1237311

Klein E.L., Guimarães S.B., Rodrigues J.B., Chaves C.L., Souza-Gaia S.M., Lopes E.C., Castro J.M.E. 2018. The Novo Progresso Formation, Tapajós Gold Province, Amazonian Craton: zircon U-Pb and Lu-Hf constraints on the maximum depositional age, reconnaissance provenance study, and tectonic implications. Journal of the Geological Survey of Brazil, 1, 31-42. https://doi.org/10.29396/jgsb.2018.v1.n1.3

Lamarão C.N., Dall'agnol R., Lafon J.M., Lima E.F. 2002. Geology, geochemistry and Pb–Pb zircon geochronology of the Paleoproterozoic magmatism of Vila Riozinho, Tapajós Gold Province Amazonian Craton, Brazil. Precambrian Research, 119, 189-223.

Law J., Phillips G. 2005. Hydrothermal Replacement Model for Witwatersrand Gold. Economic Geology. 100 Anniversary Volume, 799-811.

Lecuyer N.L., Moore C.M., 2009. Yamana Gold. Inc. Technical report on the Jacobina mine complex, Bahia State, Brazil. NI 43-101 report. Scott Wilson Roscoe Postle Associates Inc., 163 p.

Marques G.C. 2016. Mina de Jacobina: Mudanças Estratégicas para um Mercado Futuro de Ouro Jacobina Mine: Strategic Changes for a Future Gold Market. In: VII Brazilian Symposium on Mineral Exploration. Memoirs, http://www.adimb.com.br/simexmin2016/palestras/

Matsuhisa Y., Goldschmit J.R., Clayton R.N. 1979. Oxygen isotope fractionation in the system quartz-albite-anorthite-water: Geochimica et Cosmochimica Acta 43, 1131-1140.

McClenaghan M.B. 2009. Gold and PGE indicator mineral methods in mineral exploration. In: Workshop B: Indicator Mineral Methods in Mineral Exploration 24th International Applied Geochemistry Symposium.

Mello R. 2014, Mineral resources estimation for the Castelo de Sonhos Project, Pará State – Brazil: NI43-101 Technical Report, Tristar Gold Inc. www.tristagold.com

Miller C.F., Stoddard E.F., Bradfish L.J., Dollase W.A. 1981. Composition of plutonic muscovite. Canadian Mineralogist, 19, 25-34.

Minter W.E.L. 1991. Ancient placer gold deposits. In: Foster R.P. (ed.), Gold Metallogeny and Exploration. Glasgow, Blackie and Son, Ltd., p. 283-308.

Monier P., Robert J.L. 1986. Muscovite solid-solutions in the system K2O-MgO-FeO-Al2O3-SiO2-H2O: an experimental study at 2 kbar pH2O and comparison with natural Li-free white micas. Mineralogical Magazine, 50, 257-266.

Monteiro L.V.S., Xavier R.P., Souza Filho C.R., Moreto C.P.N. 2014. Metalogênese da Província Carajás. In: Silva M.G., Rocha Neto M.B., Jost H., Kuyumjian R.M. (eds), Metalogênese das Províncias Tectônicas Brasileiras. Belo Horizonte, CPRM, p. 43-92.

Omang B.O., Suh C.E., Lehmann B., Vishiti A., Chombong N.N., Fon A.N., Egbe J.A., Shemang E.M. 2015. Microchemical signature of alluvial gold from two contrasting terrains in Cameroon. Journal of African Earth Sciences, 112, 1-14. http://dx.doi.org/10.1016/j.jafrearsci.2015.09.004

Oliver N.H.S. 1996. Review and classification of structural controls on fluid flow during regional metamorphism. Journal of Metamorphic Geology, 14, 477-492.

Passchier C.W., Trouw R.A.J. 2005. Microtectonics. 2nd ed., Germany, Springer-Verlag, 366 p.

Queiroz J.D.S., Klein E.L., Rodrigues J.B. 2015. Rochas intrusivas na Formação Castelo dos Sonhos, Cráton Amazônico: petrografia, geocronologia, geoquímica e implicações para as idades de sedimentação e da mineralização no depósito aurífero Castelo de Sonhos. Boletim do Museu Paraense Emílio Goeldi, 10, 341-380.

Renger F.E., Silva R.M.P., Suckau V.E. 1988. Ouro nos conglomerados da Formação Moeda, sinclinal de Gandarela, Quadrilátero Ferrífero, Minas Gerais. In: Congresso Brasileiro de Geologia, 35, Belém, 1, 44-57.

Santos J.O.S., Groves D.I., Hartmann L.A., Moura M.A., Mcnaughton N.J. 2001. Gold deposits of the Tapajós and Alta Floresta Domains, Tapajós–Parima orogenic belt, Amazon Craton, Brazil. Mineralium Deposita, 36, 279-299.

Santos J.O.S., Van Breemen O.T., Groves D.I., Hartmann L.A., Almeida M.E., Mcnaughton N.J., Fletcher I.R. 2004. Timing and evolution of multiple Paleoproterozoic magmatic arcs in the Tapajós Domain, Amazon Craton: constraints from SHRIMP and TIMS zircon, baddeleyite and titanite U-Pb geochronology. Precambrian Research, 131, 73-109.

Schmidt V., McDonald D. A. 1979. Texture and recognition of secondary porosity in sandstones. Tulsa, Okla., Society of Economic Paleontologists and Mineralogists, Special Publication, 26, 209-225.

Sheppard S.M.F. 1986. Characterization and isotopic variations in natural waters. In: Valley J.W., Taylor H.P., O'Neil J.R. (eds.), Stable isotopes in High Temperature Geological Processes. Mineralogical Society of America, Reviews in Mineralogy, 16, 165-183.

Sibley D.F., Blatt H. 1976. Intergranular pressure solution and cementation of the Tuscarora orthoquartzite. Journal of Sedimentary Petrology, 46, 881-896.

Sibson R.H. 1994. Crustal Stress, Faulting and Fluid Flow. Geological Society of London Special Publication, 7, 869-84.

Srivastava M., Appleyard N., Pereira E., Jones M. 2016. Castelo de Sonhos: Exploration concept for a Paleoproterozoic conglomerate-hosted gold deposit. In: PDAC – Prospectors and Developers Association of Canada. Available on line at: http://www.pdac.ca/convention/programming/exploration-insights / (accessed on March 2016)

Tischendorf G., Gottesmann B., Förster H.J., Trumbull R.B. 1997. On Li-bearing micas: estimating Li from electron microprobe analyses and an improved diagram for graphical representation. Mineralogical Magazine, 61, 809-834.

Townley B.K., Hérail G., Maskaev V., Palacios C., Parseval P., Sepulveda F., Orellana R., Rivas P., Ulloa C. 2003. Gold grain morphology and composition as an exploration tool: application to gold exploration in covered areas. Geochemistry: Exploration, Environment, Analysis, 3, 29-38.

Tristar Gold. 2018. Tristar Gold Continues to Expand Resources at Castelo de Sonhos. Unpub. Report. Available on lite at: http://www.tristargold.com/index.php/news/news/2017/158-tristar-gold-continues-to-expand-resources-at-castelo-de-sonhos?tmpl=component&format=pdf / (accessed on 16 March 2018).

Vargas A.M., Campbell-Hicks C. 2017. NI 43-101 Technical Report. Mineral resource estimate update on the Castelo de Sonhos gold project, Para State, Brazil. CSA Global Canada Geosciences Ltd. Unpublished report. Available on line at: https://www.sedar.com/CheckCode.do;jsessionid=0000btKy5efrLYYI40ac5EQVVs3:188setvlh / (accessed on 2 July 2018)

Vasquez M.L., Rosa-Costa L.T., Silva C.M.G., Klein E.L. 2008. Compartimentação tectônica. In: Vasquez M.L., Rosa-Costa L.T. (eds.), Geologia e Recursos Minerais do Estado do Pará: Sistema de Informações Geográficas – SIG: Texto explicativo dos mapas Geológico e Tectônico e de Recursos Minerais do Estado do Pará, Escala 1:1.000.000: Belém, CPRM.

Vasquez M.L., Chaves C.L., Moura E.M., Araujo J.K.M. 2017. Geologia e Recursos Minerais das Folhas São Domingos - SB.21-Z-A-II e Jardim do Ouro - SB.21-Z-A-III, Estado do Pará, Escala 1:100.000. Belém: CPRM - Serviço Geológico do Brasil, 305 p.

Walker T.R. 1960. Carbonate replacement of detrital cristaline silicate minerals as a source of authigenic silica in sedimentary rocks. Geological Society of America Bulletin, 7, 145-152.

Walker T.R. 1967. Formation of red beds in modern and ancient deserts. Geological Society of America Bulletin, 85, 353-368.

Walker T.R. 1974. Formation of red beds in moist tropical climates: a hypothesis. Geological Society of America Bulletin, 85, 633-638.

Webster J.G., Mann A.W. 1984. The influence of climate, geomorphology and primary geology on the supergene migration of gold and silver. Journal of Geochemical Exploration, 22, 21-42.

Yokoi Y.O., Oliveira A.L.A.M., Tachibana J. 2001. General economic geology of the High Tapajós Basin (The "Cachimbo" Gráben) and its boundaries: a regional geological survey with exploratory purpose, in: Simpósio de Geologia da Amazônia 7, Belém. Extended abstracts, CD-ROM.

Zhang Y., Schaubs P.M., Zhao C., Ord A., Hobbs B.E., Barnicoat A. 2008. Fault-related Dilation, Permeability Enhancement, Fluid Flow and Mineral Precipitation Patterns: Numerical Models. Geological Society, London, Special Publications, 299, 239-255. https://doi.org/10.1144/SP299.15